11th World Congress on Computational Mechanics (WCCM XI)
5th European Conference on Computational Mechanics (ECCM V)
6th European Conference on Computational Fluid Dynamics (ECFD VI)
E. Oñate, J. Oliver and A. Huerta (Eds)

NUMERICAL SIMULATION OF NON-UNIFORM CORROSION STATES IN REBARS UNDER NATURAL CHLORIDE ENVIRONMENT

S. MUTHULINGAM, B. N. RAO*

Structural Engineering Division, Department of Civil Engineering
Indian Institute of Technology Madras, Chennai 600 036, India
email: bnrao@iitm.ac.in, http://www.civil.iitm.ac.in

Key Words: *Corrosion, Convection, Diffusion, Finite Element Analysis, Chloride, Concrete*.

Abstract. Corrosión of embedded rebars is a classical deterioration mechanism of reinforced concrete structures exposed to chloride environments. Macro-cell corrosion process involved in a typical chloride-induced corrosion of RC components exposed to natural chloride environment results in non-uniform corrosion states in rebars. In the present study, such non-uniform corrosión states around steel-concrete interfacs of rebars are captured by solving governing field equations through a combined finite element and finite difference scheme.

1 INTRODUCTION

Chloride-induced rebar corrosion in concrete is currently a serious problem in the world. Based on conservative estimates, one-half of highway bridges are deteriorating due to rebar corrosion in the developed countries, and billions of dollars are required to repair or rehabilitate the damaged structures. Reinforced concrete (RC) structures fail to perform their intended functions, and their service lives are much shorter than what they were designed for. Rebar corrosion is accepted as a reasonable explanation for such premature damage incurred by RC structures. Moreover, a majority of the world's population inhabit marine atmosphere (coastal) zones, the interface between the land and seawater. In such zones, salinity is the main source of built infrastructure deterioration, predominantly due to the chloride-induced rebar corrosion of the embedded steel.

The commonly considered uniform corrosion pattern around the rebar perimeter [1, 2] is quite contradictory to actual rust layer formation around rebars in concrete exposed to natural chloride environments. Owing to the spatially and temporally evolving chloride ion concentration through concrete cover thickness, and to the impermeable nature of steel bars, the rebar may not be corroding uniformly around its whole circumference. This phenomenon can be explained by the gradual chloride-induced corrosion initiation process around corner and middle rebars in a RC component exposed to natural chloride environment, as illustrated in Fig. 1.

The surface regions, around steel-concrete interfaces of rebars that are facing the external environment, where chloride accumulations are faster and higher, begin to corrode first. In a rectangular or square RC cross-section, such surface regions for corner bars are around midpoints of quadrants facing the adjacent concrete cover surfaces, and for middle bars are around shortest distances from respective concrete cover surfaces. Whereas, in steel-concrete

interfaces that are facing the interior of concrete, the amount of chloride ions remain at a very low-level because of the impermeable nature of steel bars. Hence, breakdown of surface passive protection layer and corrosion of steel could hardly happen in this area before the cracking of concrete cover. Thus, variations in the onset of corrosion reaction around steel-concrete interfaces of rebars result in non-uniform corrosion states in rebars [1, 2].

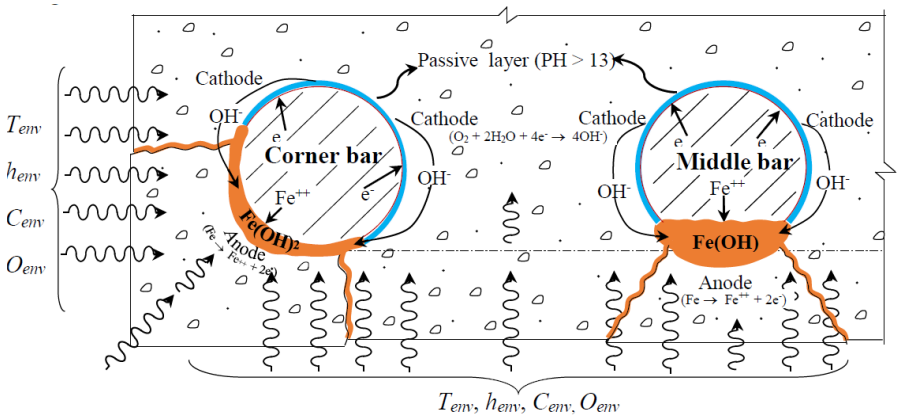

Fig. 1 Non-uniform corrosion states in corner bar and middle bar

In order to capture the non-uniform corrosion states around steel-concrete interfaces of rebars numerically, the adopted model must consider not only the existence of rebars but also their size and locations. Rebars are impermeable to the transport of moisture and chloride yet could transport heat. In addition, rebars act as obstruction to the movement of chloride ions and hence tend to could accumulate along their circumference [3]. Such accumulation could also be realized to quicken the initiation and could lead to relatively earlier onset of corrosion induced cracks. Although many approaches have been proposed to numerically model the process of chloride ingress, they either fully or partially failed to take into consideration the size and distribution of rebars.

This study is divided into three parts: (i) a single-ion approach based model that is proposed by Saetta et al. [4] which incorporates nonlinear chloride binding relationships, humidity and temperature variations is adopted to model the process of chloride ingress into RC components is dicussed; (ii) total chloride content (TCC) and time-to-corrosion initiation (TCI) evolutions around steel-concrete interface of rebars of various sizes are discussed; and (iii) based on the evaluated TCI profiles, non-uniform corrosion states are estimated by adopting empirical models.

2 CHLORIDE INGRESS MODEL

The problem of chloride ingress into concrete can be effectively studied as the interaction between three phenomena, namely: heat transport; moisture transport; and chloride transport. Each of these phenomena is represented by a partial differential equation (PDE) and their interaction is considered by solving them simultaneously. The diffusion process and the nature of chloride binding are the most important principles in modelling of chloride ingress into the concrete [6]. Subsequent subsections present each phenomenon separately, and Section 2.4 summarizes the numerical procedure to solve the whole PDE system.

2.1 Temperature transport in RC

By combining thermal equilibrium and Fourier heat law, the PDE for heat transport is given as [5]:

$$\rho c_p \dot{T} - \vec{\nabla}.(\mathrm{D}_T \vec{\nabla} T) - Q = 0 \tag{1}$$

where, ρ is density of concrete/rebar (kg/m), c_p is specific heat capacity of concrete/rebar (J/kgK), D_T is thermal conductivity of concrete/rebar (W/mK), and Q is the rate of heat generation per unit volume (W/m^3). Specific heat capacity of the rebar within the temperature range of 20–600 C is estimated from the following expression given in the literature [6] .

$$c_{p,rebar} = 425 + 7.73\times10^{-1} T_r - 1.69\times10^{-3} T_r^2 + 2.22\times10^{-6} T_r^3 \quad \text{[J/kg.°C]} \tag{2}$$

where T_r is rebar temperature (°C). The thermal conductivity of normal strength concrete is reported to depend on aggregate volume fraction, fine aggregate fraction, water/binder ratio (w/b) , temperature, and moisture condition [7]. The same can be estimated by the following expression:

$$D_{T,concrete} = D_{T,ref}\,[0.293 + 1.01\mathrm{A}_g]\times[0.8(1.62 - 1.54(w/b)) + 0.2h] \times[1.05 - 0.0025T][0.86 + 0.0036(s/a)] \quad \text{[W/m.°K]} \tag{3}$$

where h is relative humidity, s/a is fine aggregate fraction, A_g is aggregate volume fraction and $D_{T,\mathrm{ref}}$ is reference thermal conductivity (W/mK). The thermal conductivity of the rebar within the temperature range of 20–800 °C can be estimated by adopting the following expression [6]:

$$D_{T,rebar} = 54.0 - 3.33\times10^{-2} T_s \quad \text{[W/m.°K]} \tag{4}$$

However, in the normal temperature range (263.15 K $\le T \le$ 313.15 K), ρ, c_p and D_T of both the concrete and the rebar can be assumed to be constants and hence heat transfer analysis can be solved firstly without considering the influence of other mass transport processes [8, 9]. It is worth to note here that the heat flux from concrete surface to the surrounding environment and vice versa, reaches the quasi-balanced state within short time.

2.2 Moisture transport in RC

The mass conservation equation corresponding to moisture flow in concrete can be expressed in terms of the pore relative humidity gradient as shown in Eq. 5.

$$\frac{\partial w_e}{\partial h}\dot{h} - \vec{\nabla}.(D_h \vec{\nabla} h) = 0 \tag{5}$$

where w_e is evaporable water content (m^3 of water/m^3 of concrete) and D_h is relative humidity diffusion coefficient (m^2/s). The pore relative humidity diffusion coefficient, D_h depends on many factors and can be estimated in terms of reference humidity diffusion coefficient, $D_{h,ref}$ [4]:

$$D_h = D_{h,ref}\, f_h(T)\, f_h(h)\, f_h(t_e) \quad \text{[m}^2\text{/s]} \tag{6}$$

At standard temperature and pressure, adsorption isotherm relates evaporable water content and pore relative humidity. Based on thermodynamics principle of adsorption, the three parameter Braunauer-Skalny-Bodor (BSB) model gives this relationship as [10, 11]:

$$w_e = \frac{C k_c V_m h}{\left(1-k_c h\right)\left[1+\left(C-1\right)k_c h\right]} \text{ [g of water/g of cementitious material]} \quad (7)$$

Xi, Bazant and Jennings [11] developed experimental expressions for such parameters; for instance, when $t_e \geq 5$ days and $0.3 < w/b \leq 0.7$, their expressions are given as follows.

$$V_m = \left(0.068 - \frac{0.22}{t_e}\right)\left(0.85 + 0.45\frac{w}{b}\right)V_{ct},\ C = \exp\left(\frac{855}{T}\right) \quad (8–9)$$

$$k_c = \frac{\left(1-\frac{1}{n_w}\right)C-1}{C-1},\ n_w = \left(2.5+\frac{15}{t_e}\right)\left(0.33+2.2\frac{w}{b}\right)N_{ct} \quad (10–11)$$

The derivative of water content with respect to pore relative humidity (i.e., $\partial w_e/\partial h$) is defined as the moisture capacity. From the adsorption isotherm (i.e., Eq. 7), moisture capacity can be obtained by taking its derivative with respect to h:

$$\frac{\partial w_e}{\partial h} = \frac{C k_c V_m \left(C h^2 k_c^2 - h^2 k_c^2 + 1\right)}{\left(h k_c - 1\right)^2 \left(C h k_c - h k_c + 1\right)^2} \quad (12)$$

2.3 Chloride transport in RC

Chloride ingress into concrete is a complex physiochemical process. Two types of chloride ions can be present in the concrete: (i) chemically bound to the hydration products of the cement and physically sorbed on the surfaces of the gel pores (bound chlorides); and (ii) dissolved in the pore solution (free chlorides) [12, 13]. The governing PDE in terms of TCC considering both diffusion and convection transport mechanisms is given as [4, 8, 14, 15]:

$$\dot{C}_t - \underbrace{\vec{\nabla}.(D_c\, w_e\, \vec{\nabla} C_f)}_{\text{diffusion}} - \underbrace{\vec{\nabla}.(D_h\, w_e\, C_f \vec{\nabla} h)}_{\text{convection}} = 0 \text{ [Kg/m}^3\text{]} \quad (13)$$

where C_t is total chloride content (kg/m^3), D_c is effective chloride diffusion coefficient (m^2/s), and C_f is concentration of free chlorides dissolved in the pore solution (kg/m^3). If the concentrations of chemically bound and physically sorbed chlorides are grouped in the concentration of bound chlorides (kg/m^3), C_b, then TCC can be expressed as [4]:

$$C_t = C_b + w_e C_f \quad (14)$$

Using Equation 17, the governing PDE for chloride ingress can be rewritten in terms of free chloride concentration as:

$$\dot{C}_f - \underbrace{\vec{\nabla}.(D_c^a\, \vec{\nabla} C_f)}_{\text{diffusion}} - \underbrace{\vec{\nabla}.(D_h^a\, C_f \vec{\nabla} h)}_{\text{convection}} = 0 \quad (15)$$

where D_c^a is apparent chloride diffusion coefficient (m^2/s) and D_h^a apparent humidity diffusion coefficient (m^2/s). They are given as:

$$D_c^a = \frac{D_c}{1+\frac{1}{w_e}\frac{\partial C_b}{\partial C_f}} \text{ and } D_h^a = \frac{D_h}{1+\frac{1}{w_e}\frac{\partial C_b}{\partial C_f}} \quad (16–17)$$

The effect of temperature, humidity and concrete aging on D_c is estimated by modifying the reference chloride diffusion coefficient, $D_{c,ref}$ (m^2/s) measured at standard conditions [4, 8]:

$$D_c = D_{c,ref}\, f_c(T)\, f_c(t)\, f_c(h) \quad [m^2/s] \quad (18)$$

2.4 Numerical model and boundary conditions

An analytical closed form solution is very difficult to obtain for the chloride ingress model, due to the dependence of the various material properties and boundary conditions on the physical parameters of the concrete and the time level of exposure, hence numerical approach is adopted. Three PDEs are solved in space as a boundary value problem adopting two-dimensional FE model, and the evolution of spatial distribution is integrated in time as an initial value problem by using the finite difference method. Time-dependent boundary conditions, considering monthly mean variations of temperature and relative humidity are applied at the exposed boundaries as fluxes. These boundary conditions are given as:

$$X^c = \underbrace{B_c\left(C^b - C_{env}\right)}_{\text{diffusion}} + \underbrace{C_{env} X^h}_{\text{convection}} \quad (19)$$

$$X^h = B_h\left(h^b - h_{env}\right) \quad (20)$$

$$X^T = B_T\left(T^b - T_{env}\right) \quad (21)$$

Where, X^c, X^h and X^T are chloride, relative humidity and heat fluxes at the exposed boundaries respectively.B_c, B_h and B_T chloride, relative humidity and heat transfer coefficients, C^b, h^b and T^b are chloride concentration, relative humidity and temperature at the boundaries respectively.C_{env}, h_{env} and T_{env} are chloride, relative humidity and temperature in the surrounding environment.

3 PROBLEM DESCRIPTION

In the current study, TCC and TCI around the steel-concrete interfaces of rebars are estimated by considering different parameters: (i) *w*/*b* ratio (0.4,0.5, and 0.6) (ii) concrete cover thickness (25 to 75 mm in multiples of 5); and (iii) rebar diameter size (12,16, 20 and 25 mm). Furthermore, in this study, Tohoku region in Japan is considered as an example. In Japan the wind usually blows from west to east, the RC structures in Tohoku region near the Sea of Japan (East Sea) have suffered most from severe damage due to airborne chlorides [16]. In the current study, the mean monthly temperature and relative humidity data of the Tohoku region has been obtained for the last 15 years (1998 to 2012) from Japan

Meteorological Agency [17], to find the annual trend of the temperature and relative humidity.

$$T_{env}(t) = 288.9 + 11.15\sin(2\pi t) \tag{22}$$

$$h_{env}(t) = 0.70 + 0.08\sin(2\pi(t - 0.5)) \tag{23}$$

Depending on the time period of collecting airborne chlorides, it can be assumed that the total amount of surface chloride concentration due to airborne chlorides is constant within a structure's lifetime, and attenuate with distance from the coastline [18]. In the current study, RC structure is assumed to be located near the shoreline of Tohoku and hence a constant surface chloride concentration value (= 9 kg/m^3) and a critical chloride content value of 1.2 kg/m^3 of TCC reported by JSCE [19] is adopted in the numerical analysis.

For further study a RC component section of size 400 × 400 mm shown in Fig. 2a, reported is considered. In the considered cross-section: (i) C_c and d represents cover thickness and rebar diameter size respectively; and (ii) eight rebars are present of which, two bars of interest in future discussions are named B_1 (middle bar) and B_2 (corner bar). The adopted RC cross-section is discretized using four noded isoparametric quadrilateral elements as shown in Fig. 2b. In FE analysis, the input parameters are assumed as those given in Table 1.

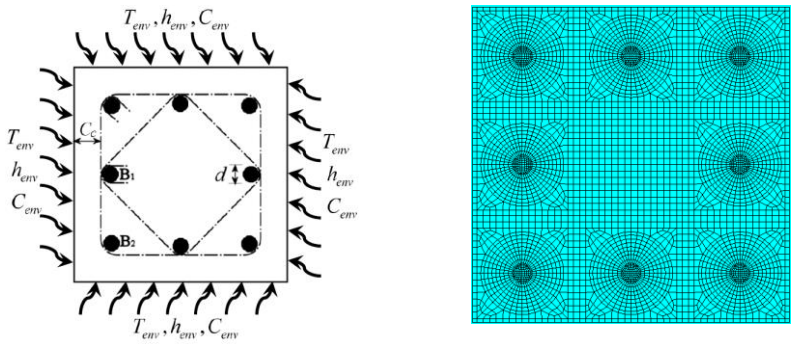

Fig. 2 Studied RC component; (a) Cross-section; (b) Finite element discretization

Table 1. Values used for numerical simulation

Heat transport	Moisture transport	Chloride transport
ρ_{concrete} = 2400 kg/m^3	α_o = 0.05	t_{ref} = 28 days
$c_{p,\text{concrete}}$ = 1000 J/kg.°K	h_c = 0.75	R = 8.314 J/mol.°K
$D_{T,\text{concrete}}$ = 2 W/m.°K	n = 10	α_L = 0.39
ρ_{rebar} = 7850 kg/m^3	m = 0.15	β_L = 0.07
$c_{p,\text{rebar}}$ = 620 J/kg.°K	t_e = 28 days	α_F = 1.05
$D_{T,\text{rebar}}$ = 50 W/m.°K	h_{ini} = 0.72	β_F = 0.36
B_T = 7.75 W/m^2.°K	B_h = 3 × 10^{-7} m/s	B_c = 1 m/s

The following section discusses the two of the three primary results obtained by considering the mathematical model and parameters explained in sections 2 and 3.

4. TCC AND TCI PROFILES

4.1 Effects of rebar location

Comparing with middle bars, more area of the steel surface of corner bars is close to the external environment because of their location. In general, TCC build up is not only faster but also higher at the steel-concrete interface around a corner bar (B_2) than that around a middle bar (B_1), as the region of chloride accumulation over the surface of a corner bar is much larger than that of a middle bar. As a result, after a certain exposure period, corner bars are observed to have higher chloride accumulation than that of middle bars. To demonstrate the effect of rebar location on chloride accumulation, a rebar size of 16 mm, three concrete cover thicknesses (30–55 mm) and a *w*/*b* (= 0.4) are considered.

Figs. 3a and b present the TCC distributions around steel-concrete interfaces of B_1 and B_2 bars after 50 years of simulation, obtained by adopting the comprehensive FE method described in section 2. The maximum TCC values of 1.01, 0.71, and, 0.47 kg/m^3 for B_1 bar and 1.54, 1.13, and, 0.78 kg/m^3 for B_2 bar are obtained for 45, 50, and, 55 mm cover thickness, respectively. These observed values indicate that, TCC build up at the steel-concrete interface is much more pronounced around a corner bar than that around a middle bar. In addition, it can be observed from Figs. 3a and b that, TCC accumulation around the steel-concrete interface that is facing the interior of concrete is much less when compared with the exterior face. Moreover, the accumulation of TCC around the steel-concrete interface that is facing the interior of concrete (Figs. 3a and b) is also higher for B_2 bar than that of B_1 bar.

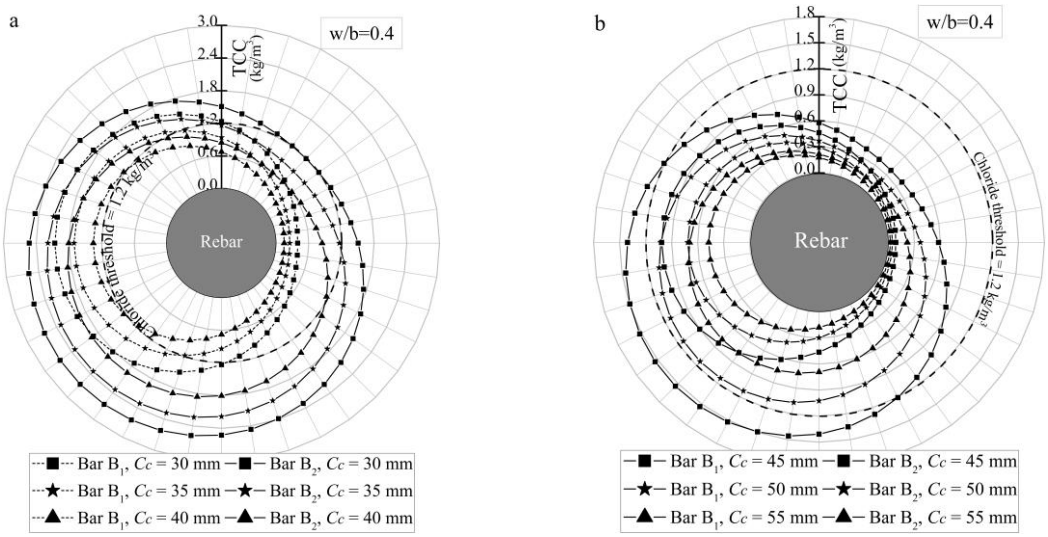

Fig. 3 TCC distributions around B_1 and B_2 bars of 16 mm diameter and 0.4 *w*/*b* ratio after 50 years for various cover thickness

4.2 Effects of rebar size

The chlorides transporting into the concrete from external aggressive environment is obstructed by the presence of steel bars, and hence starts to build up with time around steel-concrete interfaces. Such build up is observed to be higher for larger-size bars than that of smaller-size bars. To demonstrate this fact, a cover thickness value of 50 mm and a *w*/*b* ratio of 0.5 are considered. The estimated TCC distributions around steel-concrete interfaces of different rebar size (i.e., 12, 16, 20, and 25 mm) are depicted in Figs. 4a and b for B_1 and B_2 bars after 25 and 50 years of exposure to airborne chlorides, respectively. It is observed that, TCC around the steel-concrete interface that is facing the exterior of concrete increases with the increase in rebar size for B_1 bar at 25 and 50 years, and for B_2 bar at 50 years (Figs. 4a and b). However, TCC build up is observed to decrease with the increase in rebar size for B_2 bar (i.e., corner bar) at 25 years.

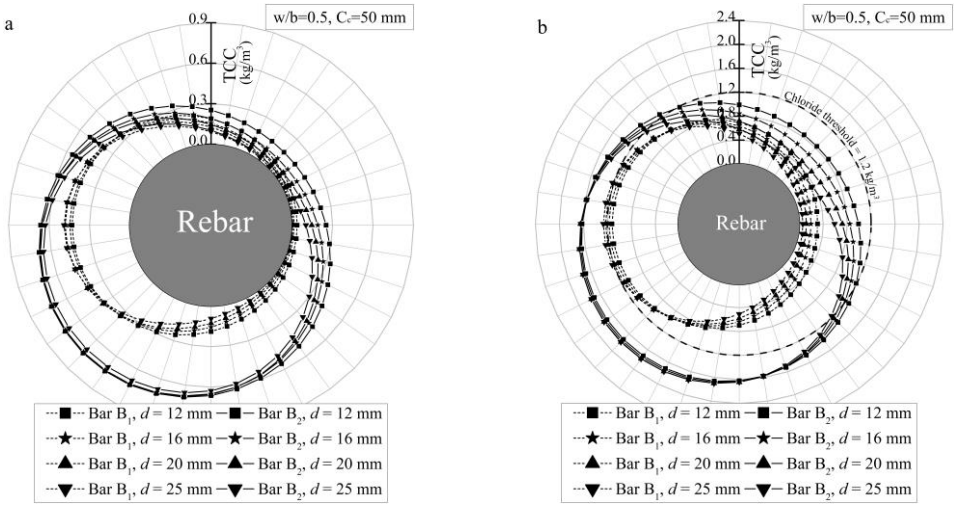

Fig. 4 TCC distributions around B_1 and B_2 bars of different diameter size; (a) 25 years; (b) 50 years

This is because the diffusion path that maximizes chloride transport from the surface of concrete to the rebar level, remain constant, and increase, with the increase in the rebar size for B_1 and B_2 bars, respectively. These criteria govern TCC build up at 25 years, and hence with the increase in the rebar size, an increase and decrease in chloride values are observed around the steel-concrete interface that is facing the exterior of concrete for B_1 and B_2 bars, respectively. However, higher chloride ions build up around the steel-concrete interface of the larger-size bar, rather than the maximizing diffusion path is observed to govern TCC distribution around B_2 bar (Fig. 4b) for longer exposure periods (say 50 years).

4.3 Time-to-corrosion initiation profiles

From the preceding section, it is observed that, TCC varies around steel-concrete interfaces of rebars. Implicit in this observation is a fact that each TCC value at the steel-concrete interface location will reach a threshold value at different exposure periods. Consequently, TCI will be different at each location of the steel-concrete interface of the rebar. The distribution of TCI values around the steel-concrete interface of the rebar, is defined in this context, as time-to-corrosion initiation (TCI) profile(s).

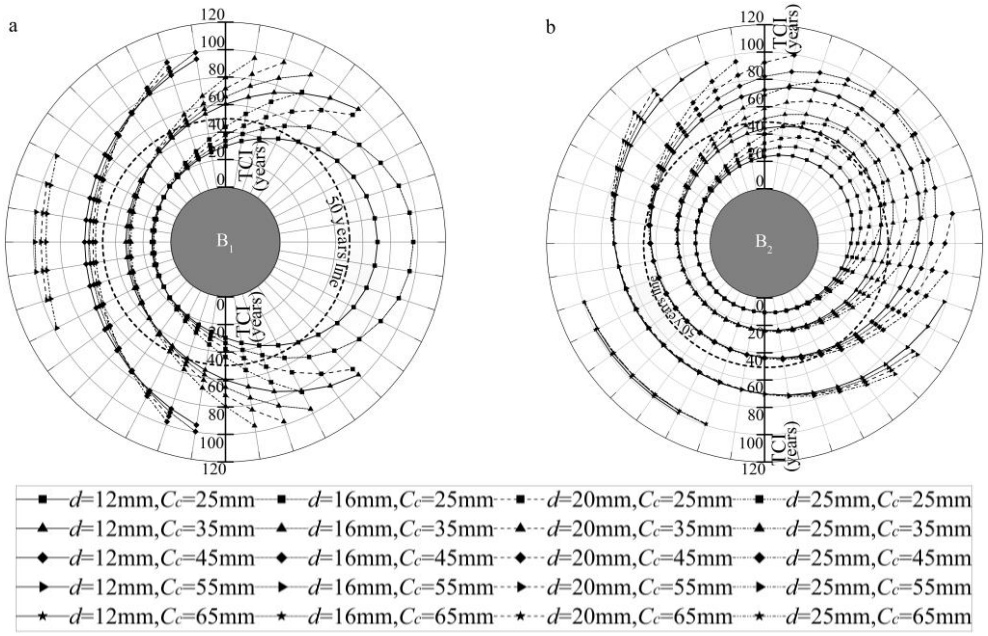

Fig. 5. TCI profiles for different combinations diameter size and concrete cover thickness; (a) middle bar; (b) corner bar

It can be observed from Figs. 5a and b that, for a given value of cover thickness and *w*/*b*, the TCI is faster for B_2 bar than that of B_1 bar. The ratio between TCI of B_1 and B_2 bar is observed to fall within the range of 1.3–1.6, indicating that, TCI is about 30 to 60% faster for B_2 bar than that of B_1 bar. Hence, the corrosion initiation and subsequent onset of cracking, as corrosion level increases over time would be much more serious in concrete around a corner rebar (i.e., B_2) than that around a middle rebar (i.e., B_1). Therefore, corner bars need more protection from external aggressive environment than middle bars.

4 NON-UNIFORM CORROSION STATES

Chloride ingress through the porous concrete cover causes localized breakdown of passive protection layer around the rebar. The ensuing localized form of corrosion is characterized by macrocell action between relatively large active steel (anode) and small passive steel (cathode). In other words, chloride induced rebar corrosion in concrete is modelled as a macrocell kind of action, in which anodic and cathodic zones on the steel surface are spatially separated [20-22]. In addition, highly localized corrosion pattern may appear due to the formation of circumferential macrocells circulating between the corroded active steel and uncorroded passive steel [23]. To numerically model macrocell corrosion, it is very essential to identify the locations of anodes (active zones) and cathodes (passive zones). The regions of steel-concrete interface in contact with the pore solution, where the chloride ion concentration is above a user-defined threshold can be considered to be anodes, while the rest of the regions act as cathodes, and thus a macrocell corrosion reaction could exist between them [24].

4.1 Corrosion rate

The rate of corrosion in concrete (corrosion rate) is one of the most important input parameters for making reasonable service life prediction in the propagation phase, as it plays a decisive role in realistic estimation of one or more of the damage procedures. Corrosion rate in RC structures is affected by various factors, namely, supplementary cementitious materials, moisture content, cyclic wetting and drying, sustained loading, loading history, concrete resistivity, concrete quality, cover depth, temperature, cracking, dissolved oxygen concentration, and exposure conditions [26]. By considering few or more of these of factors, various predictions models have been proposed in the literature. The European project DuraCrete (2000) [27] gives a following expression for estimating the corrosion rate:

$$i_{\text{corr}}(t) = i_{\text{corr-20}}[1 + k_1(T(t) - 20)] \quad [\mu\text{A/cm}^2] \tag{24}$$

where $i_{\text{corr-20}}$ is the corrosion rate at 20 °C given (=2.586 μA/cm^2 for atmospheric exposure), and k_1= 0.025 if $T(t)$< 20 C and k_1= 0.073 if $T(t)$ > 20 C.

4.2 Corrosion penetration depth

The process of rebar corrosion transforms the steel into corrosion products, leading to; (i) a reduction of the cross-sectional area; and (ii) an expansion in volume that generate splitting stresses in the cover concrete The increase in the volume of the steel eventually leads to concrete cover cracking and spalling. The corrosion level of a rebar is generally reported in terms of the depth of attack penetration. The depth of corrosion penetration would be equal and unequal around the circumference of the rebar in uniform and non-uniform corrosion states, respectively. As chloride induced rebar corrosion leads to non-uniform corrosion products layer formation around the steel-concrete interface of the bar, the penetration depth x (mm) at exposure time t (years) can be empirically estimated based on Faraday's law [28], as shown in Eq. 25.

$$x(t) = 0.0116 \int_{\text{TCI}}^{T} i_{\text{corr}}(t)\, dt \quad [\text{mm}] \tag{25}$$

By substituing Eq. 24 in Eq. 25 the time-dependent reduction in rebar cross-section can be obtained. As TCI evolve both sparially and temporally around steel-concrete interfaces of rebars, the reduction in rebar cross section would change in a similar way. Figs.9a–d display the time-dependent rebar cross-section for different cobinations of cover thickness and rebar diameter. It can be observed from these figures that reduction in cross-sectional área is much for pronounced for a corner bar tan that for a middle bar. Moreover, it can be observed from Figs.6a–d , that the cross-sectional shape of the uncorroded bar is non-uniform at any given time, in concrete exposed to natural chloride environment. In addition, such reduction in rebar cross-section would exert pressure on the nearby concrete to crack, and subsequently the cover concrete spalls off, causing reduction in cross-section área of RC member. From this quantitative represetation of non-uniform corrosión states, it can also be interpreted that cover concrete around the corner bar would suffer earlier damage that the corner bar, which could be practically observed in real structures exposed to chloride environemnt. In addition, the estimated non-uniform corrosion states qualitatively very well match the experimental observations reported in literature [6, 7].

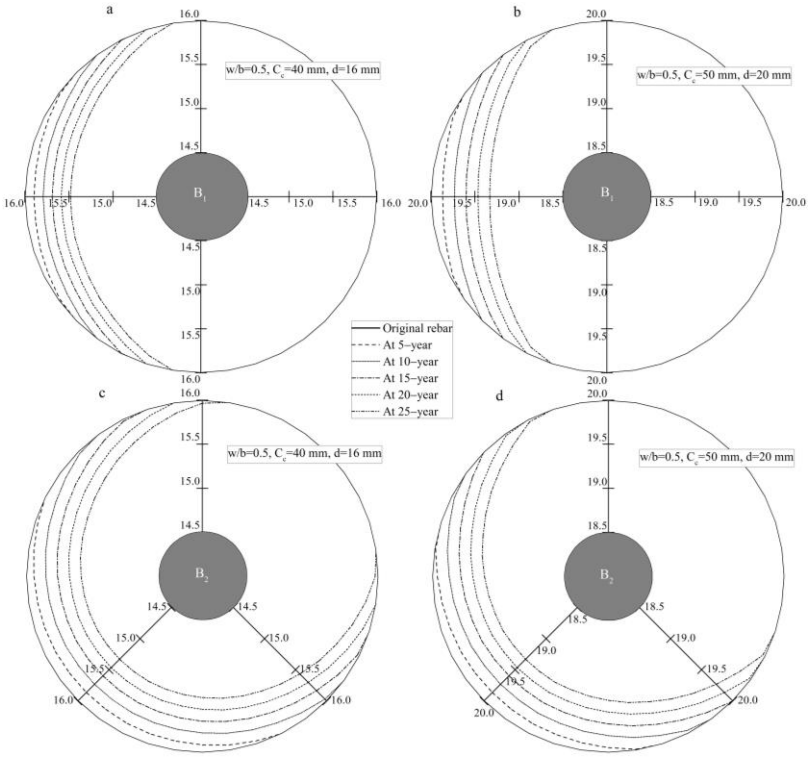

Fig. 6 Non-uniform corrosion states in rebar for various combinations of rebar diameter size and cover thickness around ;(a–b) middle bar; (c–d) corner bar

5 CONCLUSIONS

- The importance of studying the process of chloride ingress into RC by considering not only the existence of rebar but also its size and location is demonstrated through a numerical model. It is observed that TCC accumulation would be more pronounced and hence TCI would be faster for corner bar than that of the middle bar. In addition, such accumulation is also observed to increase with increase in rebar diameter size.
- Non-uniform corrosion states in rebars (i.e., non-uniform reduction in cross-section of the rebar) was evaluated based on DuraCrete empirical model. It is observed that the reduction in rebar cross-section during the corrosion propagation phase would be higher for a corner bar that that of a middle bar.

REFERENCES

[1] Y.X. Zhao, A.R. Karimi, H.S. Wong, B.Y. Hu, N.R. Buenfeld, W.L. Jin, Comparison of uniform and non-uniform corrosion induced damage in reinforced concrete based on a Gaussian description of the corrosion layer, Corrosion Science, 53 (2011) 2803–2814.

[2] N. Xia, Q.W. Ren, R.Y. Liang, J. Payer, A. Patnaik, Nonuniform corrosion-induced stresses in steel-reinforced concrete, ASCE Journal of Engineering Mechanics, 138 (2012) 338–346.

[3] B.H. Oh, B.S. Jang, Chloride diffusion analysis of concrete structures considering effects of reinforcements, ACI Materials Journal, 100 (2003) 143–149.

[4] A.V. Saetta, R.V. Scotta, R.V. Vitaliani, Analysis of Chloride Diffusion into Partially Saturated Concrete, ACI Materials Journal, 90 (1993) 441–451.

[5] Z.P. Bazant, L.J. Najjar, Nonlinear water diffusion in nonsaturated concrete, Matériaux et Constructions, 5 (1972) 3–20.
[6] Eurocode 3, Design of steel structures, Part 1-2: General rules - Structural fire design, BS EN 1993-1-2, 2005.
[7] K.H. Kim, S.E. Jeon, J.K. Kim, S.C. Yang, An experimental study on thermal conductivity of concrete, Cement and Concrete Research, 33 (2003) 363–371.
[8] B. Martin-Perez, S.J. Pantazopoulou, M.D.A. Thomas, Numerical solution of mass transport equations in concrete structures, Computers & Structures, 79 (2001) 1251–1264.
[9] O. Burkan Isgor, A.G. Razaqpur, Finite element modeling of coupled heat transfer, moisture transport and carbonation processes in concrete structures, Cement and Concrete Composites, 26 (2004) 57–73.
[10] S. Brunauer, J. Skalny, E.E. Bodor, Adsorption on non-porous solids, Journal of Colloid and Interface Science, 30 (1969) 546–552.
[11] Y.P. Xi, Z.P. Bazant, H.M. Jennings, Moisture diffusion in cementitious materials - adsorption-isotherms, Advanced Cement Based Materials, 1 (1994) 248–257.
[12] L.P. Tang, L.O. Nilsson, Chloride binding-capacity and binding isotherms of opc pastes and mortars, Cement and Concrete Research, 23 (1993) 247–253.
[13] A. Neville, Chloride attack of reinforced-concrete - an overview, Materials and Structures, 28 (1995) 63–70.
[14] D.V. Val, P.A. Trapper, Probabilistic evaluation of initiation time of chloride-induced corrosion, Reliability Engineering & System Safety, 93 (2008) 364–372.
[15] E. Bastidas-Arteaga, A. Chateauneuf, M. Sanchez-Silva, P. Bressolette, F. Schoefs, A comprehensive probabilistic model of chloride ingress in unsaturated concrete, Engineering Structures, 33 (2011) 720–730.
[16] M. Akiyama, D.M. Frangopol, I. Yoshida, Time-dependent reliability analysis of existing RC structures in a marine environment using hazard associated with airborne chlorides, Engineering Structures, 32 (2010) 3768–3779.
[17] Japan Metereological Agency, http://www.data.jma.go.jp/obd/stats/data/en/normal/normal.html.
[18] M. Akiyama, D.M. Frangopol, M. Suzuki, Integration of the effects of airborne chlorides into reliability-based durability design of reinforced concrete structures in a marine environment, Structure and Infrastructure Engineering, 8 (2012) 125–134.
[19] JSCE, Standard Specification for Concrete Structures (Maintenance), Society of Civil Engineers, Tokyo, Japan, 2007.
[20] C. Andrade, I.R. Maribona, S. Feliu, J.A. Gonzalez, S. Feliu, The Effect of Macrocells between Active and Passive Areas of Steel Reinforcements, Corrosion Science, 33 (1992) 237–249.
[21] L. Bertolini, P. Pedeferri, T. Pastore, B. Bazzoni, L. Lazzari, Macrocell effects on potential measurements in concrete cathodic protection systems, Corrosion, 52 (1996) 552–557.
[22] B. Elsener, Macrocell corrosion of steel in concrete - implications for corrosion monitoring, Cement & Concrete Composites, 24 (2002) 65–72.
[23] C.Y. Kim, J.K. Kim, Numerical analysis of localized steel corrosion in concrete, Construction and Building Materials, 22 (2008) 1129–1136.
[24] O.B. Isgor, A.G. Razaqpur, Advanced modelling of concrete deterioration due to reinforcement corrosion, Canadian Journal of Civil Engineering, 33 (2006) 707–718.
[25] M. Otieno, H. Beushausen, M. Alexander, Prediction of corrosion rate in reinforced concrete structures - a critical review and preliminary results, Materials and Corrosion, (2011).
[26] M.B. Otieno, H.D. Beushausen, M.G. Alexander, Modelling corrosion propagation in reinforced concrete structures - A critical review, Cement & Concrete Composites, 33 (2011) 240–245.
[27] DuraCrete. 2000. Probabilistic calculations. DuraCrete—probabilistic performance based durability design of concrete structures. EU—brite EuRam III. Contract BRPR-CT95-0132. Project BE95-1347/R12-13. May 2000. p. 41.
[28] J. Rodriguez, L.M. Ortega, J. Casal, J.M. Diez, Corrosion of reinforcement and service life of concrete structures, in: Durability of Building Materials and Components 7, Stockholm, 1996, pp. 117–126.